Computers and Structures 87 (2009) 1366–1373

Contents lists available at ScienceDirect

Computers and Structures

journal homepage: www.elsevier.com/locate/compstruc

Craters produced by underground explosions

Bibiana Luccioni [a,*], Daniel Ambrosini [b], Gerald Nurick [c], Izak Snyman [d]

[a] Structures Institute, National University of Tucumán, CONICET, Av. Roca 1800, 4000 S.M. de Tucumán, Argentina
[b] Engineering Faculty, National University of Cuyo. CONICET, Centro Universitario – Parque Gral., San Martín – 5500 Mendoza, Argentina
[c] Blast Impact and Survivability Research Unit (BISRU), Department of Mechanical Engineering, University of Cape Town, Rondebosch 7701, South Africa
[d] Landward Sciences, DPSS, CSIR, P.O. Box 395, Pretoria, South Africa

ARTICLE INFO

Article history:
Received 1 December 2008
Accepted 1 June 2009
Available online 16 July 2009

Keywords:
Crater
Blast load
Soil
Hydrocode

ABSTRACT

Extensive research activities in the field of blast loads have taken place in the last few decades. There are many experimental results related to underground explosions. The mechanism of crater formation is complex and it is related to the dynamic physical properties of air, soil and air/soil interface. Studies concerned with the characteristics of craters caused by explosions usually resort to dimensional analysis and statistics. Some empirical equations proposed for the evaluation of crater dimensions can be found in the literature. Nevertheless, they were obtained for particular type of soils, shapes of explosives, ranges of explosive mass and depth of explosive and they present considerable variability.

The main objective of this paper is to prove the accuracy of numerical simulation of craters produced by underground explosions. For this purpose, the numerical analysis of crater formation due to underground explosions is performed with a hydrocode. Several numerical approaches are carried out using different models and processors for the soil. Moreover, different alternatives for the constitutive model of the soil are used.

Comparison with experimental results is performed in order to validate the numerical approach and prove its ability to model the crater formation. Many simulations of the same physical model lead to the same crater dimensions and a good agreement between the test results and the predicted crater measures is achieved.

1. Introduction

Tests of crater formation are appropriate tools to study the blast phenomena, the behavior and destructive power of different explosives and the response of soils and rocks under this type of load (Persson et al. [1]). The mechanism of crater formation is complex and it is related to the dynamic physical properties of air, soil and air/soil interface. Even very carefully performed cratering tests give deviations in the dimensions measured of about 10%, while differences of as much as 30–40% are common (Bull and Woodford [2]).

A cavity is always formed when a confined explosion is produced in a mass of soil. If the explosion is close to the surface, a crater is formed, a complex interaction taking place between gravity effects, soil strength and transient load conditions. The most important variables in defining the crater shape and size are the mass W of the explosive and the depth of the detonation beneath the air/soil interface d. When $d < 0$, the explosive is detonated over the air/soil interface, $d = 0$ when the detonation occurs in the air/soil interface and $d > 0$ when the explosive is detonated beneath the soil surface. For $d > 0$, the crater mechanism is altered by gravitational effects. When the depth of the detonation increases, larger amounts of subsoil must be expelled by the explosion. Thus the crater radius and the depth of the crater increase when d increases, until a certain limit value, from which they rapidly decrease (Bull and Woodford [2]).

Studies concerned with the characteristics of craters caused by explosions usually resort to dimensional analysis and statistics. The scaling law establishes that any linear dimension L of the crater can be expressed as a constant multiplied by W^{α} divided by the distance of the charge from the ground, where W represents the equivalent TNT mass of explosive and α is a coefficient depending on if the gravitational effects can be neglected or not. In the first case the cubic root law is applicable ($\alpha = 0.33$) and in the other cases the functional dependence can be quite complex.

Baker et al. [3] present a dimensional study to model the crater formation phenomenon in the case of underground explosions. Six parameters are chosen to define the problem: the explosive mass W, the depth of the explosive charge d, the apparent crater radius R, the soil density ρ, and two strength parameters to define the soil

* Corresponding author. Tel./fax: +54 381 4364087.
E-mail addresses: bluccioni@herrera.unt.edu.ar.edu.ar (B. Luccioni), dambrosini@uncu.edu.ar (D. Ambrosini), Gerald.Nurick@uct.ac.za (G. Nurick), isnyman@csir.co.za (I. Snyman).
URLs: http://www.herrera.unt.edu.ar/iest (B. Luccioni), http://www.fing.uncu.edu.ar/estructural/index.html (G. Nurick).

0045-7949/$ - see front matter © 2009 Published by Elsevier Ltd.
doi:10.1016/j.compstruc.2009.06.002

properties: one with the dimensions of a stress σ, related to soil strength, and the other, K, with the dimensions of a force divided by a cubic length (Nm^{-3}) that takes into account gravitational effects.

After a dimensional analysis and many empirical observations, the following functional relation may be obtained [3]

$$\frac{R}{d} = f\left(\frac{W^{7/24}}{\sigma^{1/6}K^{1/8}d}\right) \quad (1)$$

If $\frac{R}{d}$ (scaled radius of the crater) is plotted as a function of $W^{7/24}/d$, it can be seen that this relation is close to experimental results and can be approximately simplified by two straight lines, one with a moderate slope for $W^{7/24}/d > 0.3$ and one steeper for $W^{7/24}/d < 0.3$. For $W^{7/24} < 0.3$, the scaled radius of the crater is sensible to small changes in the independent parameter and, due to this fact, the independent parameter or the scaled radius may exhibit great variability. Experimental conditions are better controlled for $W^{7/24} > 0.3$.

It can be deduced that the specific weight ρg is the best measure for K and that ρc^2 is the best measure for σ, where c is the seismic velocity in the soil. If experimental results for different types of soils are plotted in a $\frac{R}{d}$ versus $\frac{W^{7/24}}{\rho^{7/24}c^{1/3}g^{1/8}d}$ graph, it may be clearly seen that there is very little variability in the results.

The numerical evaluation of the dimensions of craters produced by underground cylindrical TNT loads is presented in this paper. Although there are many experimental results and empirical equations for the size of craters produced by underground explosions, the main objective of this paper is to check the ability of numerical tools to reproduce experimental values in order to use these tools for more complex problems such as the evaluation of damage produced on vehicles or objects situated on the ground by underground explosions.

The analysis is performed with a hydrocode (AUTODYN v6.1 [4]). Many alternative models for the same problem are first run in order to check the variability of the results. Then the dimensions of the craters for different TNT masses and depths are obtained and compared with experimental values. The crater dimensions defined by Kinney and Graham [5] are used in this work (Fig. 1). D is the apparent crater diameter measured from the loose soil mounts around the crater, D_r is the actual crater diameter and H_2 is the apparent depth of the crater.

2. Problem description

2.1. Introduction

First a typical problem is chosen in order to study the variability obtained in craters dimensions when different processors, different mesh sizes and slightly different physical models are used. Once these aspects have been checked, the mass and depth of the explosive are varied, maintaining all the other properties, and the resulting craters dimensions are compared with experimental and empirical values.

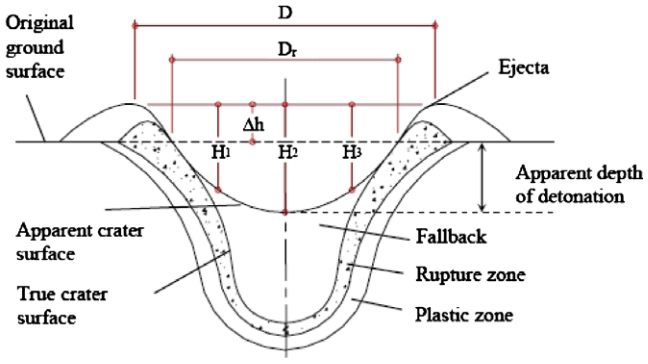

Fig. 1. Definitions of the crater dimensions.

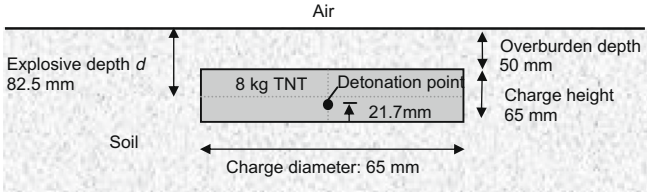

Fig. 2. Typical problem set-up.

2.2. Explosive

In order to carry out a comparable analysis, the mass of the explosive is defined by TNT masses. The corresponding masses for other explosives can be obtained through the concept of TNT equivalence (Formby and Wharton [6]).

A mass of 8 kg of TNT is defined for the typical problem and then the mass is varied from 0.26 to 8 kg of TNT.

A cylindrical explosive load like that represented in Fig. 2 is considered for all the problems. The dimensions of the TNT load for the typical problem are also indicated in Fig. 2. For the other problems the TNT mass is varied preserving the shape and the aspect ratio of the explosive load.

The explosive charge includes a Pentolite booster with a hole for the detonator at one third of the height from the lower face of the TNT cylindrical charge.

2.3. Soil

All the results are obtained for a ferricrete, gravelly sand soil with the properties presented in Table 1 for two different depths. The plasticity index of soil, that is, the difference between the plastic and the liquid limit, indicates the size of the range over which the material acts as a plastic – capable of being deformed under stress, but maintaining its form when unstressed.

2.4. Location

For the typical problem the cylindrical charge is buried with top surface 50 mm below the soil level. The charge is covered up to the ground level with loose soil (no strength). The set-up is graphically displayed in Fig. 2.

Problems varying the depth of the explosive load were also studied.

The detonation point is considered to be placed in the center of the lower face of the explosive load as indicated in Fig. 2. Nevertheless, the variation of results for other positions of the detonation point is also studied.

3. Numerical models

3.1. Introduction

Computer codes normally referred as "hydrocodes" encompass several different numerical techniques in order to solve a wide

Table 1
Soil properties.

Depth (mm)	Dry density (g/cm^3)	Plasticity index
150	1.987	4
300	2.071	5

variety of non-linear problems in solid, fluid and gas dynamics. The phenomena to be studied with such a program can be characterized as highly time dependent with both geometric and material non-linearities. Different numerical tools are used in some papers in order to solve similar problems of crater determination. For example ABAQUS (Yang et al. [7]), AUTODYN (Wu et al. [8], Wang and Lu [9]), SALE2D (Baratoux and Melosh [10], Nolan et al. [11]) and CTH (Pierazzo and Melosh [12]).

In this paper, the software AUTODYN v6.1 [4], which is a "hydrocode" that uses finite-difference, finite volume, and finite element techniques to solve a wide variety of non-linear problems in solid, fluid and gas dynamics, is used. The various numerical processors available in AUTODYN generally use a coupled finite-difference/finite volume approach similar to that described by Cowler and Hancock [13]. The first-order Euler approach scheme is based upon the method developed by Hancock [14].

While finite element codes are usually based on the equilibrium condition, the hydrocode uses the differential equations governing unsteady material dynamic motion: the local conservation of mass, momentum and energy. In order to obtain a complete solution, in addition to appropriate initial and boundary conditions, it is necessary to define a further relation between the flow variables. This can be found in a material model, which relates stress to deformation and internal energy (or temperature). In most cases, the stress tensor may be separated into a uniform hydrostatic pressure (all three normal stresses equal) and a stress deviatoric tensor associated with the resistance of the material to shear distortion.

The relation between the hydrostatic pressure, the local density (or specific volume) and local specific energy (or temperature) is known as an equation of state. Since solids are able to withstand a certain amount of tensile stress, it is necessary to consider extending the equations of state into limited regions of negative values of the pressure (tension). However, since the analytic forms derived for ranges of positive pressure may not be valid for extrapolation into the negative regions special attention should be paid in using some forms of equation of state. The hydrodynamic tensile limit, sometimes referred to as p_{min}, is the minimum pressure at which the material can sustain continuous expansion. If the material pressure drops below this limit in a cell it is assumed that the material will fracture, or in some way lose its uniform and continuous ability to sustain a tensile pressure. This would then be the lower limit of the analytic equation of state. Regardless the definition of a value of $p_{min,}$ it may be necessary to provide a different analytic form for negative pressure values from the one used for positive values (but taking care to ensure continuity of function and derivatives at $p = 0$).

While there are many problems that can be calculated using a hydrodynamic equation of state, there are many applications where material strength effects (i.e. its resistance to shearing forces) cannot be ignored and indeed may even dominate. If the material is solid and has finite shear strength then, in addition to the calculation of the hydrostatic pressure, it is necessary to define relations between shear stress and strain. The methodology followed in this paper is the first one formulated by Wilkins [15] to extend conventional numerical hydrodynamic codes to include the effects of material strength and resistance to shear distortion.

A relation to define the transition between elastic and plastic strain, both in compression and release, and a relation to define the onset of fracture, are also required. The yield criterion governing the transition from elastic to plastic behaviour may involve only constant yield strength, or this strength may itself be a function of the degree of strain (work hardening), the rate of strain and/or the temperature of the material (energy dependency).

Real materials are not able to withstand tensile stresses that exceed the material local tensile strength. The computation of the dynamic motion of materials assuming that they always remain continuous, even if the predicted local stresses reach very large negative values, will lead to unphysical solutions. For this reason the model has to be constructed to recognize when tensile limits are reached, to modify the computation to deal with this and to describe the properties of the material after this formulation has been applied.

Many alternative numerical models for the same physical problem were run, analyzed and compared. The alternatives that gave comparable and more reliable results are described in the following sections.

First, the effect of the size and refinement of the numerical mesh was studied. Different meshes were analyzed from a fine mesh with 332,500 to the coarsest mesh with 67,200 cells for the complete problem. The mesh was refined in air and soil near the explosive charge where the crater was expected to be formed. The cells dimensions varied from 5 mm to 20 mm in the finest

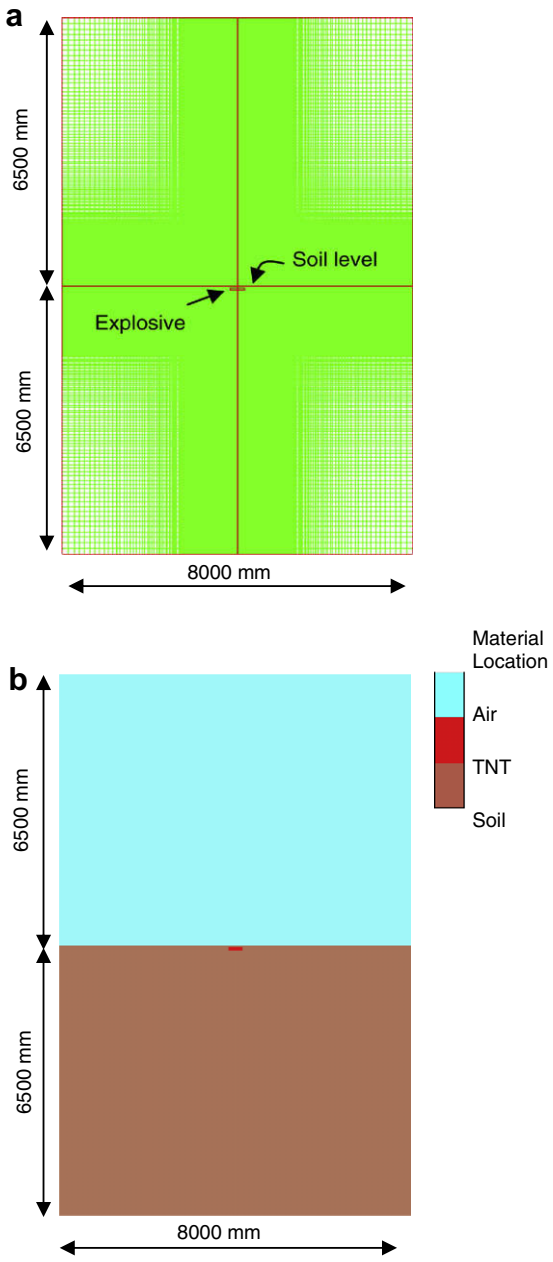

Fig. 3. Numerical model. Cross section through the charge center. (a) Numerical mesh; and (b) different materials in the model.

mesh, while for the coarsest mesh the cells dimensions varied from 10 mm to 50 mm. The mesh presented in Section 3.2 was adopted based on the convergence of these results.

Different numerical processors, Euler and Lagrange, were used to model the soil. The models and results obtained are presented in Sections 3.2 and 4, respectively.

Moreover, different alternatives for the constitutive model of the soil were used.

3.2. Numerical mesh and processors

The symmetry conditions allow using a two-dimensional (2D) mesh considering axial symmetry. A 13 m × 4 m mesh with a minimum 10 mm × 10 mm size was used. This mesh represents an 8 m-diameter cylinder.

The mesh used for the typical problem is shown in Fig. 3a. The mesh was filled with different materials: air, TNT and soil, indicated with different colors in Fig. 3b.

A previous estimation of the final diameter and depth of the crater has been made and the mesh was refined with 10 mm cell all around the estimated final crater. Then, the maximum error in the final diameter of the crater is 20 mm and the maximum error in the depth is 10 mm.

The following two alternative models using different numerical processors for the soil were compared.

(a) In this model an Euler Godunov multi material with strength higher order processor is used to model the complete problem including the air, the explosive charge and the soil.

(b) In this model an Euler Godunov processor is used to model the air and the explosive charge while a Lagrange processor is used for the soil. Coupling between Euler and Lagrange processors together with an erosion algorithm for the soil were defined in this case.

In AUTODYN the integral and discrete forms of the problem equations are expressed in conservation form to obtain accurate, stable solutions. Terms producing changes in conserved variables are divided into two groups: Lagrangian or transport (convective). A two-step numerical procedure is used to solve the finite-difference equations. In the first step, the Lagrange step, the Lagrangian form of the equations are updated or advanced one time interval (time step). In the second step, the Euler step, the updated variables are mapped onto the Euler mesh. Multiple materials are handled through either a volume fraction technique or an interface technique originally developed by Youngs [16]. All variables are cell centered. This allows arbitrary shaped control volumes to be formed more readily at the interface between Euler and Lagrange grids, facilitating the computation of fluid-structure or gas-structure interaction problems.

3.3. Material models

3.3.1. Air

The ideal gas equation of state was used for the air. This is one of the simplest forms of equation of state for gases. In an ideal gas, the internal energy is a function of the temperature alone and if the gas is polytropic the internal energy is simply proportional to temperature. It follows that the equation of state for a gas, which has uniform initial conditions, may be written as,

$$p = (\gamma - 1)\rho e \tag{2}$$

in which p is the hydrostatic pressure, ρ is the density and e is the specific internal energy. γ is the adiabatic exponent, it is a constant (equal to $1 + R/c_v$) where constant R may be taken to be the universal gas constant R divided by the effective molecular weight of the particular gas and c_v is the specific heat at constant volume. The values of the constants used for air are presented in Table 2.

Table 2
Air properties.

Equation of state for air: ideal gas
$\gamma = 1.4$
Reference density: $\rho_a = 1.225 \times 10^{-3}$ g/cm^3
Reference temperature: $T_0 = 288.2$ K
Specific heat: $c_v = 717.3$ J/kg K

3.3.2. TNT

An explosion may be initiated by various methods. However, initiation of an explosive always goes through a stage in which a shock wave is an important feature. Lee–Tarver equation of state (Lee and Tarver [17]) was used to model both the detonation and expansion of TNT in conjunction with "Jones–Wilkins–Lee" (JWL EOS) to model the unreacted explosive.

The (JWL) equation of state can be written as,

$$p = C_1\left(1 - \frac{\omega}{r_1 v}\right)e^{-r_1 v} + C_2\left(1 - \frac{\omega}{r_2 v}\right)e^{-r_2 v} + \frac{\omega e}{v} \tag{3}$$

where $v = 1/\rho$ is the specific volume, C_1, r_1, C_2, r_2 and ω (adiabatic constant) are constants and their values have been determined from dynamic experiments and are available in the literature for many common explosives. The values used for TNT are presented in Table 3.

It can be shown (AUTODYN [4]) that at large expansion ratios the first and second terms on the right hand side of Eq. (3) become negligible and hence the behaviour of the explosive tends towards that of an ideal gas. Therefore, at large expansion ratios, where the explosive has expanded by a factor of approximately 10 from its original volume, it is valid to switch the equation of state for a high explosive from JWL to ideal gas. In such a case the adiabatic exponent for the ideal gas, γ, is related to the adiabatic constant of the explosive, ω, by the relation $\gamma = \omega + 1$. The reference density for the explosive can then be modified and the material compression will be reset. Potential numerical difficulties are therefore avoided.

3.3.3. Soil

A Mie–Gruneisen form of equation of state based on the shock Hugoniot was used (AUTODYN [4]). The Rankine–Hugoniot equations for the shock jump conditions can be regarded as defining a relation between any pair of the variables ρ, p, e, u_p (material velocity behind the shock) and U (shock velocity). In many dynamic experiments (AUTODYN [4]) it has been found that for most solids and many liquids over a wide range of pressure there is an empirical linear relationship between u_p and U.

$$U = c_0 + s u_p \tag{4}$$

in which c_0 is the initial sound speed and s a dimensionless parameter.

This is the case even up to shock velocities around twice the initial sound speed c_0 and shock pressures of order 100 GPa (AUTODYN [4]). In this case the equation of state is:

Table 3
TNT properties.

Equation of state for TNT: JWL
Reference density $\rho = 1.658$ g/cm^3
$C_1 = 3.7377 \times 10^8$ kPa
$C_2 = 3.73471 \times 10^6$ kPa
$R_1 = 4.15$
$R_2 = 0.9$
$\omega = 0.35$
C–J detonation velocity: 6.93×10^3 m/s
C–J energy/unit volume: 6×10^6 KJ/m^3
C–J pressure: 2.1 10^7 kPa

$$p = p_H + \Gamma\rho(e - e_H) \quad \text{with} \quad p_H = \frac{\rho_0 c_0^2 \mu(1+\mu)}{[1-(s-1)\mu]^2}; \quad e_H = \frac{1}{2}\frac{p_H}{\rho_0}\frac{\mu}{1+\mu}; \quad \mu = \frac{\rho}{\rho_0} - 1 \tag{5}$$

where p is the hydrostatic pressure, $\rho_{\bar{0}}$ is the initial density, e is the specific internal energy and Γ is the Gruneisen Gamma parameter and it is assumed that $\Gamma_\rho = \Gamma_0\rho_0 = const$.

A Drucker Prager strength criterion with piecewise hardening and hydro tensile limit (100 kPa) was used for the strength effects of the soil in the Euler model. The same strength and failure models were used for the Lagrange model but an erosion limit was added. An erosion criterion based on instantaneous geometric strain (erosion limit = 0.5) was used. The initial density was taken as $\rho = 2.2$ g/cm^3 (wet density). The wet density was obtained considering a mean dry density of 2100 kg/m^3 and a moisture content of 5%.

For non-cohesive soils, it could be necessary to use shear modulus varying with depth. In absence of SPT data or other useful data such us Dynamic Cone Penetration Tests or Field Vane Test, a medium shear modulus in all depth was used.

A summary of soil properties used for all the models is presented in Table 4.

It is important to note that it was previously proved (Ambrosini et al. [18]) that the influence of the soil properties on the size of craters produced by explosive loads is usually rather small (variations of about ±5% in crater diameter could be obtained).

Many analysis using different constitutive models have been performed and similar crater dimensions were obtained.

In a recent paper [19] it was also proved that the type of soil and the model used have practically non influence in the diameter of the crater produced by buried explosions. It should be noted that this conclusion can not be extrapolated to the propagation of blast waves in soils. It was also proved by the authors in Ref. [19] that blast wave propagation in soils is strongly dependent on the type of soil modeled and the model used. Consequently, in order to assess the effect of buried explosions on underground structures, the soil properties and model should be more carefully studied and defined [19–22].

Many alternatives for the loose soil over the explosive charge were simulated: a soil with the same properties of the rest of the soil, a soil with reduced strength and stiffness (one half mass density and an order of magnitude minor shear elasticity modulus were used) and non soil but air over the explosive charge.

3.4. Boundary transmit

In order to fulfill the radiation condition, a transmitting boundary was defined for air as well as soil subgrids external limits. The transmit boundary condition allows a stress wave to continue "through" the physical boundary of the subgrid without reflection. The size of the numerical mesh can be reduced by use of this boundary condition. The transmit boundary is only active for flow out of a grid. Nevertheless, there is actually some wave reflection on transmit boundaries. The dimensions of the grid have been chosen in order to guarantee that for the range of blast charges studied (1–10 kg of TNT) reflections on transmit boundaries could be neglected.

The transmit boundary is calculated as follows:

Let the normal velocity at the boundary be U_n, where U_n is positive for outflow. Then the boundary pressure (P) is computed as follows:

For $U_n > 0$

$$P = P_{ref} + (U_n - U_{ref})I \tag{6}$$

For $U_n < 0$:

$$P = P_{ref} \tag{7}$$

in which P_{ref} and U_{ref} are the pressure and velocity of reference respectively (material model properties) and I is the material impedance (density soundspeed). If the impedance at the boundary is undefined, it is taken from values in adjacent cells.

Table 4
Properties for soil model.

Equation of state for soil: shock strength model for soil: Drucker Prager
Reference density $\rho = 2.2$ g/cm^3
Gruneisen Gamma $\Gamma = 0.11$
$c_o = 1.614 \times 10^3$ m/s
$S = 1.5$
Shear Modulus $G = 2.4 \times 10^5$ kPa
Pressure 1 = -1.149×10^3 kPa Yield stress 1 = 0 kPa
Pressure 2 = 6.88×10^3 kPa Yield stress 2 = 6.2×10^3 kPa
Pressure 3 = 1.0×10^{10} kPa Yield stress 3 = 6.2×10^3 kPa
Hydro tensile limit $p_{min} = -100$ kPa

4. Numerical and experimental results for the typical problem

First, the results obtained for both models described for the typical problem are presented. According to a previous paper (Ambrosini and Luccioni, [23]), the mechanical properties of the soil do not significantly affect the diameter of the crater obtained. However, a variation of ±5% could be obtained in the crater diameter.

A larger model than those found in other papers and works in the literature was used. This model allows checking when the explosive wave is far away from both the air and the soil. The problem has been run until the crater dimensions remained stable.

In other works, a time of approximately 20 ms from the detonation instant has been determined as enough to obtain the final dimensions of the crater (Ambrosini et al. [24]; Ambrosini et al. [18]; Ambrosini and Luccioni [23]).

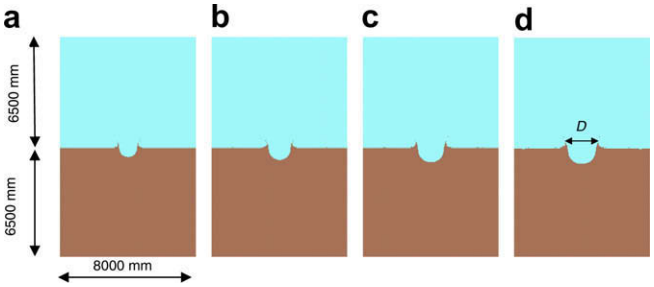

Fig. 4. Crater formation sequence obtained with an Euler processor for the soil. Cross section. (a) $t = 3$ ms; (b) $t = 6$ ms; (c) $t = 12$ ms; and (d) $t = 17$ ms.

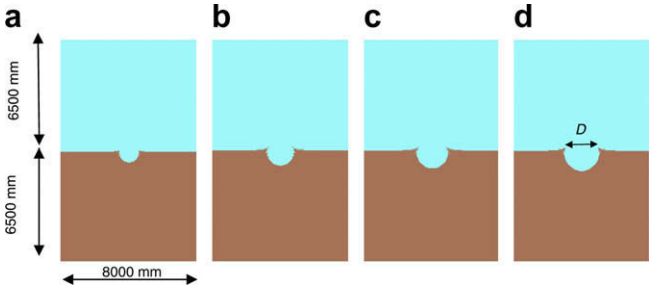

Fig. 5. Crater formation sequence obtained with a Lagrange processor for the soil. Cross section. (a) $t = 3$ ms; (b) $t = 6$ ms; (c) $t = 12$ ms; and (d) $t = 17$ ms.

Fig. 6. The 8 kg TNT charge before the soil cover.

Fig. 7. The crater with strung lines to measure the depth.

4.1. Euler processor: Model a

The final state of the model is presented in Fig. 4. The apparent diameter of the crater obtained is $D = 2070$ mm.

4.2. Euler processor: Model b

The final state of the model is presented in Fig. 5. The apparent diameter of the crater obtained is $D = 2060$ mm.

Table 6
The dimensions of the crater.

Averaged between tests #1, #2 and #3		Standard deviation (mm)	Range (mm)
Apparent crater diameter D (mm)	1898	46	87
Actual crater diameter D_r (mm)	1597	38	70
Depth H_2 (mm)	443	55	100
Depth H_1 (mm)	306	17	33
Depth H_3 (mm)	300	26	50

4.3. Other alternatives simulated

The results obtained for the crater diameter of the typical problem, varying the properties of the soil and the position of the detonation point are coincident with those presented in previous sections.

4.4. Experimental results and comparison

Three field tests were conducted, each with an 8 kg TNT cylindrical charge, at the Detonics, Blast and Explosion Laboratory (DBEL) at Paardefontein Test Range, South Africa. A schematic of the field test set-up is shown in Fig. 2. In Fig. 6 the 8 kg TNT charge for test 1 is shown before it was covered with 50 mm of soil. The charge has a 320 mm diameter to height ratio of 5–1. A 100 g Pentolite booster is caste in the centre to facilitate detonation.

Before positioning of each charge, the centre of the recess in the soil is determined by lining up three strings of about 4 m each, marking their locations with pegs. This is to facilitate the measuring of the crater dimensions afterwards. The detonator is inserted in the centre from above to a depth of two thirds through the height of the charge. Loose soil is then used to cover the charge. After the charge has been detonated, the size of the crater is measured. The crater from test 1 is shown in Fig. 7 with the three strings replaced in position after the blast. The experimental results are presented in Tables 5 and 6.

The apparent crater diameter measured as 1898 mm agrees with the crater diameter of 2065 mm calculated by AUTODYN. The difference obtained of about 9% is very small for this type of studies considering the uncertainties involved.

It should be noted that since the shape of the crater is determined by a complex sequence of events, deviations from Fig. 1 in physical appearance will occur. For instance, the loose soil between the vertical measure H_1 (at position A in Fig. 7 and Fig. 8) and the side of the crater is most probably blown out very early in the event, yielding a plateau close to the edge. The final effect is the appearance of a secondary crater inside the larger crater (see

Table 5
Crater dimensions of each test.

Test	Measurement point #	Outer diameter D (mm)	Inner diameter D_r (mm)	Depth H_2 (mm)	Depth H_1 (mm)	Depth H_3 (mm)	Height Δh (mm)
Test #1	1	1950	1700	470	300	270	50
	2	1900	1500	470	310	290	100
	3	2000	1670	470	290	250	70
	Average	1950	1623	470	300	270	73
Test #2	1	1800	1470	380	292.5	320	80
	2	1890	1570	380	310	300	35
	3	1900	1620	380	275	340	70
	Average	1863	1553	380	293	320	62
Test #3	1	1750	1480	480	325	310	50
	2	1890	1660	480	315	320	65
	3	2000	1700	480	335	300	45
	Average	1880	1613	480	325	310	53

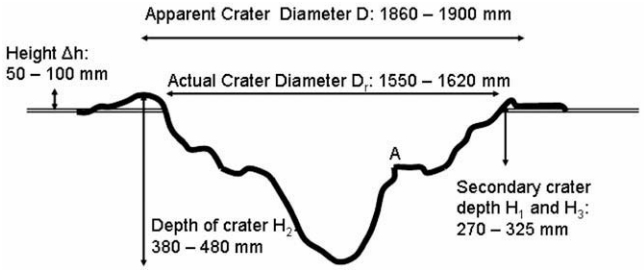

Fig. 8. An average profile of the crater based on the three field tests.

Fig. 8). However, this physical appearance did not affect the vertical measurements H_1, H_2 or H_3.

5. Variation of crater diameter with scaled distance

The diameter of the craters produced by different TNT masses located at different depths are obtained in this section. The results for different scaled distances are presented in Table 7 and Fig. 9 where d represents the distance from the explosive charge mass center to the soil surface. The numerical results were obtained with a model similar to model a, using an Euler processor. A cylindrical explosive load of 0.26 or 8 kg of TNT was used and depth was varied. The mesh was always refined in the surroundings of the explosive charge.

Comparison of experimental (DBEL) and numerical results presented in this paper with experimental and numerical results previously obtained by the authors and other authors is also shown in Fig. 9. Experimental results presented by Baker et al. [3] correspond to craters produced by explosions in alluvium soils. Experimental results by Ambrosini et al. [25] correspond underground explosions in reddish brown clayey silt of low plasticity. Spherical charges equivalent to 1, 2, 4, 7 and 10 kg of TNT were situated 500 mm below ground level. The experimental results by Fišerová [26] represent width of craters caused by the explosions of 100 g C-4 cylindrical charges in dry sand with 0 mm, 30 mm and 80 mm overburden. On the other side, numerical result by Lu et al. [21] represents the crater diameter produced by 50 kg of TNT spherical blast load at 4800 mm below ground level and was also obtained with AUTODYN [4] but with a different soil model.

Table 7
Crater diameter for different TNT masses and depths.

Mass of explosive BW (kg of TNT)	Depth d (mm)	$W^{7/24}/d$ ($kg^{7/24}$/mm)	Crater diameter D (mm)
8	0.032	0.00048	2020
8	0.082	0.00067	2070
8	0.20	0.00112	2600
8	0.50	0.00400	3120
0.26	0.60	0.01000	1270
0.26	1.00	0.02223	920
0.26	1.40	0.06150	700

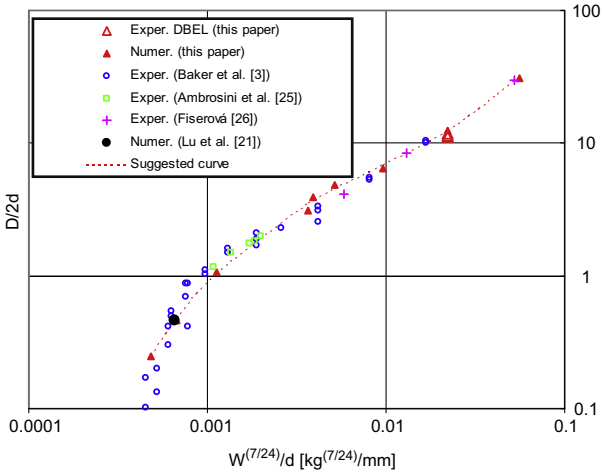

Fig. 9. Variation of crater diameter with scaled distance. Comparison with experimental results.

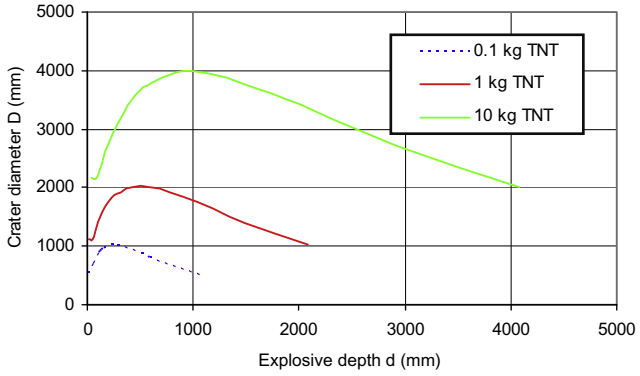

Fig. 10. Variation of crater diameter with overburden for different TNT masses.

Although the types of soils involved and the shape of the explosive load are different, an excellent agreement between the present numerical results and those corresponding to Baker et al. [3], Ambrosini et al. [25], Fišerová [26] and Lu et al. [21] can be observed in Fig. 9. The present numerical results confirm that a function relating $D/2d$ and $W^{7/24}/d$ can be established. The tendency curve that best describes the numerical is also presented in Fig. 9 with a dot line. This curve can be described by Eq. (8).

$$\log(D/2d) = 0.2993\left(\frac{W^{7/24}}{d}\right)^3 + 1.8562\left(\frac{W^{7/24}}{d}\right)^2 + 4.49130.2993\left(\frac{W^{7/24}}{d}\right) + 4.7946 \quad (8)$$

The variation of crater diameters with explosive depth obtained with Eq. (8) for different amounts of TNT is represented in Fig. 10. It is clear that an optimum depth for which the crater is maximum can be defined and this value depends on the explosive mass. This result is coincident with the experimental observations [27] for blast craters in rock.

6. Conclusions

A very good agreement is observed between the crater diameter obtained with an Euler processor for the soil (model a) and that obtained with a Lagrange processor (model b). The crater obtained with model b is deeper than that obtained with model a. In both cases, it is clear that the obtained depth is greater than the apparent depth observed in an experimental test (see Fig. 1). The final shape of the crater obtained with model a better resembles the actual one than that obtained with model b.

It has been proved that the effect of the loose soil above the explosive and the position of the pentolite booster practically do not influence the final crater diameter.

A good agreement in crater diameter with experimental results obtained by other researchers and the authors has been obtained. The shape of the explosive load and the type of soil have practically

no influence on the value of the crater diameter. This conclusion is supported by Fig. 9 where the crater diameters produced in different soils by different explosive charge shapes (cylindrical with different aspect ratio and spherical) were plotted showing the same tendency. It is clear that these results cannot be extrapolated for sheet explosives near the soil surface for which results would probably differ. Moreover, Fig. 9 and Eq. (8) are valid for explosive materials other than TNT, but it must be taken into account that W refers to TNT equivalent mass.

It is important to note that the software used gives the possibility of finding the rupture and plastic zones of the crater. In order to use the results given by the software related to rupture and plastic zones, a more detailed study of the soil model and soil properties used should be carried out, because they will obviously influence those results. Erosion limit used in Lagrange simulations has been found to be an important point to study because not only the dimensions of the rupture zone but also the stability of the numerical solution strongly depends on this value. Erosion criterion is a numerical procedure to avoid great deformation when Lagrange processor is used for the soil. In this sense, it is related to mesh size and the authors could verify that it is not completely arbitrary. If a high value of erosion limit was chosen interface overlapping occurred and the simulation was aborted. The value used for the erosion limit was the maximum admissible value to prevent interface overlapping for this particular problem.

Using this value for the erosion limit in the Lagrange processor resulted in a crater with practically the same diameter than that obtained with the Euler processor. Nevertheless, the influence of the erosion limit value in relation to the Lagrange mesh size should be subject of further research.

Acknowledgements

The authors wish to thank the programme manager Mr. D. Reinecke and the Detonics, Explosives, Ballistics Laboratory Test team, of the CSIR, that executed the test series and the help received from Mrs. Amelia Campos for the English revision. The financial support of the CONICET (Argentina), CIUNT (National University of Tucumán) and SECYT (National University of Cuyo) is gratefully acknowledged.

References

[1] Persson PA, Holmberg R, Lee J. Rock blasting and explosives engineering. USA: CRC Press; 1994.
[2] Bull JW, Woodford CH. Camouflets and their effects on runway supports. Comput Struct 1998;69(6):695–706.
[3] Baker WE, Westine PS, Dodge FT. Similarity methods in engineering dynamics. Amsterdam: Elsevier; 1991.
[4] AUTODYN, Explicit software for non-linear dynamics, version 6.1, user's manual. Century Dynamics Inc.; 2005.
[5] Kinney GF, Graham K. Explosive shocks in air. 2nd ed. Springer-Verlag; 1985.
[6] Formby SA, Wharton RK. Blast characteristics and TNT equivalence values for some commercial explosives detonated at ground level. J Hazard Mater 1996;50:183–98.
[7] Yang R, Bawden WF, Katsabanis PD. A new constitutive model for blast damage. Int J Rock Mech Min Sci Geomech Abstr 1996;33(3):245–54.
[8] Wu C, Lu Y, Hao H. Numerical prediction of blast-induced stress wave from large-scale underground explosion. Int J Numer Anal Meth Geomech 2004;28:93–109.
[9] Wang Z, Lu Y. Numerical analysis on dynamic deformation mechanism of soils under blast loading. Soil Dyn Earthquake Eng 2003;23:705–14.
[10] Baratoux D, Melosh HJ. The formation of shatter cones by shock wave interference during impacting. Earth Planet Sci Lett 2003;216:43–54.
[11] Nolan MC, Asphaug E, Greenberg R, Melosh HJ. Impacts on asteroids: fragmentation, regolith transport and disruption. Icarus 2001;153:1–15.
[12] Pierazzo E, Melosh HJ. Hydrocode modeling of Chicxulub as an oblique impact event. Earth Planet Sci Lett 1999;165:163–76.
[13] Cowler MS, Hancock SL. Dynamic fluid-structure analysis of shells using the PISCES 2DELK computer code. In: Fifth international conference on structural dynamics in reactor technology, paper B1/6; 1979.
[14] Hancock S. Finite difference equations for PISCES-2DELK, TCAM-76-2. Phys Int 1976.
[15] Wilkins ML. Calculation of elastic–plastic flow. Meth Comput Phys 1964;3:211–63.
[16] Youngs DL. Time-dependent multimaterial flow with large fluid distortion. Numer Meth Fluid Dynam 1982.
[17] Lee EL, Tarver CM. Phenomenological model of shock initiation in heterogeneous explosives. Phys Fluid 1980;23(12):2362–72.
[18] Ambrosini D, Luccioni B, Danesi R. Influence of the soil properties on craters produced by explosions on the soil surface. Comp Mech 2004;XXIII:571–90.
[19] Luccioni B, Ambrosini R. Effect of buried explosions. Comp Mech 2007;XXVI:2656–73.
[20] Wang ZQ, Hao H, Lu Y. A three-phase soil model for simulating stress wave propagation due to blast loading. Int J Numer Anal Meth 2004;28(1):33–56.
[21] Lu Y, Wang Z, Chong K. A comparative study of buried structure in soil subjected to blast load using 2D and 3D numerical simulations. Soil Dynam Earthquake Eng 2005;25:275–88.
[22] Wang Z, Lu Y, Hao H, Chong K. A full coupled numerical analysis approach for buried structures subjected to subsurface blast. Comput Struct 2005;83:339–56.
[23] Ambrosini D, Luccioni B. Craters produced by explosions on the soil surface. J Appl Mech, ASME 2006;736:890–900.
[24] Ambrosini D, Luccioni B, Danesi R. Craters produced by explosions on the soil surface. Comput Mech 2003;XXII:678–92.
[25] Ambrosini D, Luccioni B, Danesi R, Riera J, Rocha M. Size of craters produced by explosive charges on or above the ground surface. Shock Waves 2002;12(1):69–78.
[26] Fišerová D. Numerical analyses of buried mine explosions with emphasis on effect of soil properties on loading. Ph.D. Thesis, Defence College of Management and Technology, Cranfield University; 2006.
[27] Tu-qiang YE. Field experiment for blasting crater. J China Univ Mining Technol 2008;18(2):224–8.